THE EFFECT OF RADIAL POROSITY OSCILLATION ON THE HEAT TRANSFER PERFORMANCE IN PACKED BED LATENT HEAT STORAGE SYSTEM

Hongbing Liu[1], Yao Zhao[1] and Changying Zhao[1]

[1] Institute of Engineering Thermophysics, Shanghai Jiao Tong University, Shanghai (China)

Abstract

The porosity of the packed bed latent heat storage (LHS) system oscillates in the radial direction, leading to the non-uniformity of the flow field, which further affects the heat transfer and heat storage performances at different locations. In this paper, a three-dimensional packed bed LHS system model is established. The reason for radial porosity oscillation is revealed by intercepting a series of cylindrical surfaces along the radial direction, and the model is verified by experimental data. The numerical results show that the radial velocity distribution of the heat transfer fluid (HTF) and the radial temperature distribution of the phase change material (PCM) are consistent with the radial porosity distribution. The liquid fraction change of the PCM over time in the radial direction indicates that the PCM melts faster at locations with higher porosity. In addition, the effect of different aspect ratios on the flow, heat transfer and heat storage in the packed bed LHS system are studied. The radial porosity of the packed beds with different aspect ratios shows different distributions, and the closer to the center position, the greater the difference. Furthermore, the flow velocity of the HTF near the wall is faster with larger aspect ratio, which results in a faster heat transfer and heat storage rate of the PCM capsules at the near wall region. As the aspect ratio increases, the charging time can be greatly reduced, and the average charging power can be also improved, but the pressure drop within the packed bed increases rapidly.

Keywords: latent heat storage, three-dimensional packed bed, radial porosity, liquid fraction, aspect ratio

1. Introduction

Due to the reduction of traditional energy reserves and the requirement of environmental protection, the proportion of renewable energy utilization continues to increase. Solar energy has the advantages of clean, safe, and inexhaustible, and utilization methods mainly include photovoltaic power generation and solar thermal utilization. However, solar energy is intermittent, which requires the energy storage technology to ensure its stable operation. In solar thermal utilization, latent heat storage has the characteristics of large energy density, stable operation temperature and technical maturity (Zhao et al., 2018). The application of latent heat storage can greatly reduce the volume of the heat storage tank, thereby reducing the construction cost (Zhang et al., 2016). In the design of heat storage tank, the heat transfer efficiency of the packed bed is higher than that of the traditional shell-and-tube heat exchanger (Li et al., 2018b). On the one hand, the diameter of PCM capsules is usually several tens of millimeters, so capsules have shorter heat transfer distances (Alam et al., 2015); on the other hand, since the HTF flows directly through the gaps between the PCM capsules, the packed bed has a larger heat exchange area (Anderson et al., 2015). Therefore, the packed bed LHS system has a great potential in solar thermal utilization. The researches on the packed bed LHS system include numerical simulation and experimental research. Numerical simulation can provide important guidance for experimental research, and thus has been widely studied. However, some assumptions and the calculation methods used in previous numerical studies did not apply to the packed bed model. For example, the porosity in a packed bed was considered to be uniform (Zhao et al., 2017). In fact, there exists a wall effect in the packed bed, and the porosity will oscillate in the radial direction, especially near the wall (Mueller, 2005). The ratio of the tank diameter (D_{tank}) to the PCM capsule diameter (d_p), known as the aspect ratio, is an important parameter for evaluating the oscillation trend. When the aspect ratio is less than 10, the oscillation of the radial porosity will be more prominent (Freund et al., 2003). Although some relevant studies have considered the change of radial

doi:10.18086/swc.2019.22.06 Available at http://proceedings.ises.org

porosity, the representative element volume (REV) method was used (Bellan et al., 2015). But each representative element volume cannot represent the information in the region, especially at the capsule's surface where the HTF exchanges heat with the capsule. Therefore, the REV method cannot reflect the heat transfer between the PCM capsules, and is no longer suitable for the scale. Therefore, based on the actual packing process of capsules, a three-dimensional packed bed LHS model is established, and the influences of radial porosity distribution and different aspect ratios on flow, heat transfer and heat storage performances in the packed bed LHS system are further studied.

2. Modelling

2.1 Physical model

The three-dimensional packed bed model is established in an open source software *Blender*. The *Blender* software embeds Python scripts, and the Bullet Physics Library allows it to calculate the collision and friction between rigid bodies under the gravity field (Partopour and Dixon, 2017). In the modelling process, a cylindrical container is first built by programing in *Blender*, then small capsules are continuously generated above the container to fall. After all the capsules have finished falling, the establishment of the three-dimensional packed bed model is completed. The radial porosity distribution of a three-dimensional packed bed model is compared with that of Mueller's work and the corresponding aspect ratio is 7.99 (Mueller, 1992). In Fig. 1, it can be observed that the two curves both oscillate and match well with the other one, which proves the reliability of the established model. Besides, the change of radial porosity in the packed bed also indicates that the internal porosity cannot be simply assumed to be uniform, further proving the necessity of establishing a three-dimensional packed bed model.

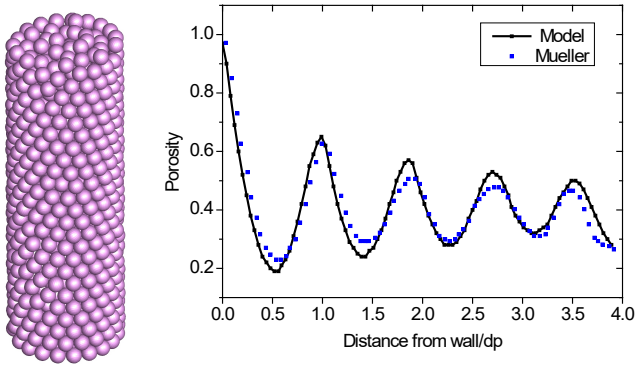

Fig.1: Comparison of radial porosity distributions when aspect ratio = 7.99

In the packed bed, the contact type between the capsules is point contact, which is not conducive to the meshing process. In order to solve this problem, there are four methods to deal with contact points: overlaps, gaps, caps, and bridges, as shown in Fig.2. Studies have shown that the bridges method can obtain the best results in the situation with heat transfer (Dixon et al., 2013). Therefore, after completing the packing process of the capsules in *Blender*, the coordinates of the capsules are obtained to calculate the distance and the unit vector of each two capsules. Then small cylinders are inserted as heat bridges in the middle of two capsules, and the diameter of the small cylinder is dp/10. The effect of the addition of the small cylinders on the average porosity of the packed bed is 0.05%-0.08%. As for the treatment of the contact points between the capsules and the container wall, the gaps method is adopted. After enlarging the diameter of the container by 1 mm, a narrow gap is formed between the capsules and the container wall.

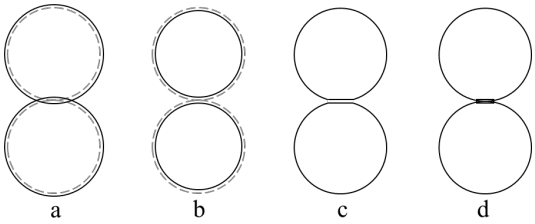

Fig. 2: Methods to deal with contact points: a) overlaps, b) gaps, c) caps, d) bridges

Li et al. (2018a) built a packed bed LHS system filled with 385 PCM capsules, and the aspect ratio was 7.65. The PCM in the capsules is ternary carbonate Li_2CO_3-K_2CO_3-Na_2CO_3 (32–35–33wt%), and its thermal properties are shown in Tab. 1. According to the experiment details, a physical model is constructed as shown in Fig. 4. The extended inlet part and outlet part are added to eliminate the influence of the inlet and outlet on the packed bed part as much as possible. The charging time of the system is defined as the time when the central temperature in the PCM capsule at the outlet position reaches 1K lower than the inlet temperature. The PCM temperature evolutions at different heights during charging process are selected to verify the correctness of the three-dimensional packed bed LHS model. During charging process, the initial temperature T_0 of the packed bed is 598.15K. The inlet is the mass flow inlet boundary condition, $T_{in} = 738.15\text{K}$, $q_{in} = 260\text{kg}\cdot\text{h}^{-1}$, and the outlet is the pressure outlet boundary condition, $P_{out} = 101325\text{Pa}$. When calculating the total heat storage and heat storage efficiency of the packed bed LHS system, the heat stored in the capsule shell and the container tank in the form of sensible heat is also considered.

Tab.1: Thermal properties of PCM

PCM	Tm/°C	ΔH/kJ kg^{-1}	λ/W m^{-1} K^{-1}	Cp/J kg^{-1} K^{-1}	ρ/kg m^{-3}
Li_2CO_3-K_2CO_3-Na_2CO_3 (32–35–33wt%)	395.1	273.0	1.69(s); 1.60(l)	1540(s); 1640(l)	2310

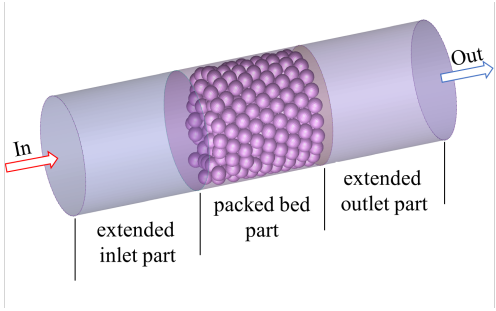

Fig. 3: Schematic diagram of three-dimensional packed bed LHS system

2.2 Mathematical model

2.2.1 Assumptions

(1) The effect of gravity on HTF flow is ignored;

(2) The convection effect of the PCM in the capsules is ignored;

(3) Radiation heat transfer of the HTF and the PCM capsules is ignored.

2.2.2 Governing equation for HTF

In the packed bed LHS system, the Reynolds number based on mean velocity is defined as (Gunjal et al., 2005):

$$\text{Re}_p = \frac{\rho(u_{in}/\varphi)d_p}{\mu} \qquad \text{(eq. 1)}$$

Where φ represents the average porosity of the packed bed, it is calculated from the volume of the PCM capsules and the volume of the container and φ = 0.426. The Reynolds number in the packed bed LHS system is calculated as Re_p=3053.61, so the flow is turbulent flow (Eppinger et al., 2011). Considering that the heat transfer surface of the PCM capsule is spherical, and in order to enhance the wall treatment, the flow model of the HTF is RNG k-ε turbulence model. Then the governing equation of HTF in the packed bed LHS system can be written in the following format (Argyropoulos and Markatos, 2015):

Continuity equation:

$$\frac{\partial\rho}{\partial t} + \frac{\partial(\rho u_i)}{\partial x_i} = 0 \qquad \text{(eq. 2)}$$

Momentum equation:

$$\frac{\partial}{\partial t}(\rho u_i)+\frac{\partial}{\partial x_j}(\rho u_i u_j)=-\frac{\partial p}{\partial x_i}+\frac{\partial}{\partial x_j}\left[\mu\left(\frac{\partial u_i}{\partial x_j}+\frac{\partial u_j}{\partial x_i}-\frac{2}{3}\delta_{ij}\frac{\partial u_i}{\partial x_j}\right)-\left(\rho\overline{u_i'u_j'}\right)\right] \quad \text{(eq. 3)}$$

Energy equation:

$$\frac{\partial}{\partial t}(\rho E)+\frac{\partial}{\partial x_i}(\rho u_i E)=\frac{\partial}{\partial x_i}\left[\left(\lambda+\frac{c_p\mu_t}{\sigma_T}\right)\frac{\partial T}{\partial x_j}+u_i(\tau_{ij})_{\text{eff}}\right] \quad \text{(eq. 4)}$$

K equation:

$$\frac{\partial}{\partial t}(\rho k)+\frac{\partial}{\partial x_i}(\rho k u_i)=\frac{\partial}{\partial x_j}\left[\left(\mu+\frac{\mu_t}{\sigma_k}\right)\frac{\partial k}{\partial x_j}\right]+G_k-\rho\varepsilon \quad \text{(eq. 5)}$$

ε equation:

$$\frac{\partial}{\partial t}(\rho\varepsilon)+\frac{\partial}{\partial x_i}(\rho\varepsilon u_i)=\frac{\partial}{\partial x_j}\left[(\mu+\frac{\mu_t}{\sigma_\varepsilon})\frac{\partial\varepsilon}{\partial x_j}\right]+C_{1\varepsilon}\frac{\varepsilon}{k}G_k-C_{2\varepsilon}\rho\frac{\varepsilon^2}{k}-R_\varepsilon \quad \text{(eq. 6)}$$

Where the turbulent viscosity μ_t, the generation of turbulence kinetic energy G_k and the additional term R_ε are given by (Yakhot and Smith, 1992):

$$\mu_t=\rho C_\mu\frac{k^2}{\varepsilon} \quad \text{(eq. 7)}$$

$$G_k=\mu_t\left(\frac{\partial u_i}{\partial x_j}+\frac{\partial u_j}{\partial x_i}\right)\frac{\partial u_j}{\partial x_i} \quad \text{(eq. 8)}$$

$$R_\varepsilon=\frac{C_\mu\rho\eta^3(1-\eta/\eta_0)}{1+\beta\eta^3}\cdot\frac{\varepsilon^2}{\beta} \quad \text{(eq. 9)}$$

$$\eta=Sk/\varepsilon\ ,\ S=\sqrt{2S_{ij}S_{ij}}\ ,\ S_{ij}=\frac{1}{2}(\frac{\partial u_i}{\partial x_j}+\frac{\partial u_j}{\partial x_i}) \quad \text{(eq.10)}$$

The constants in above equations are C_μ= 0.0845, $C_{1\varepsilon}$=1.42, $C_{2\varepsilon}$=1.68, η_0=4.38, β=0.012。

2.2.2 Governing equation for PCM in the capsules

For PCM in the capsules, since the internal natural convection is neglected, the energy equation can be expressed as (Xia et al., 2010):

$$\frac{\partial}{\partial t}(\rho_{\text{pcm}}H_{\text{pcm}})-\nabla\cdot(\lambda_{\text{pcm}}\nabla T_{\text{pcm}})=0 \quad \text{(eq.11)}$$

Where H_{pcm} represents the enthalpy of PCM, defined as the sum of sensible heat and latent heat:

$$H_{\text{pcm}}=h_{0,\text{pcm}}+\int_{T_0}^{T_{\text{pcm}}}C_{\text{p, pcm}}\text{d}T_{\text{pcm}}+\Delta H \quad \text{(eq.12)}$$

Where $h_{0,\text{pcm}}$ is the enthalpy of PCM at the initial temperature. $\triangle H$ represents the latent heat released of PCM during the charging process, defined as $\Delta H=\beta L$. L is the latent heat of PCM, and β is the liquid fraction of PCM. β can be written as following at different temperatures:

$\beta=0$, while $T_{\text{pcm}}<T_{\text{s}}$ (eq.13)

$\beta=1$, while $T_{\text{pcm}}>T_{\text{l}}$ (eq.14)

$$\beta=\frac{T_{\text{pcm}}-T_{\text{s}}}{T_{\text{l}}-T_{\text{s}}},\ \text{while}\ T_{\text{s}}\le T_{\text{pcm}}\le T_{\text{l}} \quad \text{(eq.15)}$$

Where T_{pcm}, T_0, T_s, T_l represent the temperature of the PCM, the initial temperature, the onset melting temperature and the ending melting temperature, respectively.

2.3 Meshing and validation

Since there are hundreds of PCM capsules randomly filled in the packed bed, unstructured grids are adopted to generate the mesh. The shrink-wrap method is used to generate the surface mesh, after which the volume is filled with the polyhedral meshes (Partopour and Dixon, 2017). In this process, the mesh quality is optimized to above 0.3. In grid-independent verification, the maximum grid size of the PCM capsule is set to dp/12, dp/14, dp/16 and dp/18, and the pressure drop at the inlet and outlet, as well as the charging time of the packed bed LHS system are calculated. In Figure 5, it can be seen that as the maximum mesh size decreases, the pressure drop of the inlet and outlet increases first and then stabilizes, while the charging time is first reduced and then stabilized. Therefore, the grid size of dp/18 is selected for the mesh generation.

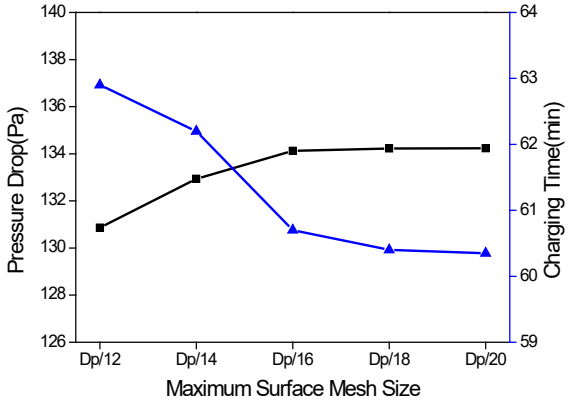

Fig.5: Grid-independence verification

Li et al. (2018a) tested the temperature evolutions of the PCM capsules along the height direction z/H = 0.25, 0.5, 0.75, as shown in Figure 6a. In order to verify the reliability of the three-dimensional packed bed LHS system model established in this paper, the simulation results are compared with the experimental data, as shown in Figure 6b. It can be obtained that the simulation results of the model at the three locations agree well with the experimental data, and the results at z/H=0.75 match the best. However, the simulation results at z/H=0.25 are faster than the experimental results, and there are two reasons for this. First, the process of promoting the inlet temperature from 598.15K to 738.15K in the calculation is completed in a short time, while the temperature change in the experiment requires a certain heating time, so the temperature rise of the calculation model is faster than that of the experiment at the beginning. Second, the influence of the inlet temperature change has a greater impact on the PCM capsules near the inlet, therefore the PCM capsule near the outlet shows better results. In general, the comparison between calculation and experimental results validates the reliability and effectiveness of the three-dimensional packed bed LHS system model.

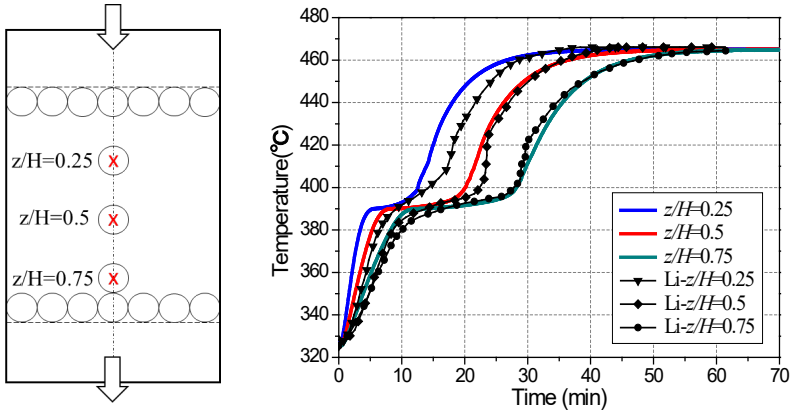

a b

Fig. 6: a) schematic diagram of packed bed LHS experiment system; b) comparison of calculation results with experimental data

3. Results and discussion

3.1 Flow analysis

For the packed bed LHS system model with the aspect ratio of 7.65, the variation of the radial porosity is shown in Fig.7b, and in order to show it more intuitively, several cylindrical surfaces at different radial positions inside the packed bed model are intercepted, as shown in Fig.8. The distance of the a-h cylindrical surfaces from the tank wall are 0, 0.5dp, dp, 1.44dp, 1.88dp, 2.32dp, 2.76dp, 3.24dp, respectively. The solid area on the cylindrical surface represents the HTF, and the white area represents the PCMs in the capsules. Therefore, the ratio of the HTF area to the whole surface area on each cylindrical surface is the porosity of that radial position, and it can be seen that the porosity of the cylindrical surfaces a, c, e, g is higher than that of cylindrical surfaces b, d, f, h. And the reason for the oscillating distribution of the radial porosity inside the packed bed is related to the process of packing capsules and the spherical shape of the capsules. Take the bottom view of the packed bed for illustration, as shown in Figure 7a. During the packing process, capsules tend to fill the space close to the wall first, and then fill the space in the center (Mueller, 2010). Therefore, the arrangement of the capsules near the wall will be regular, and the arrangement of the capsules at the tank center will be somewhat random. At the wall surface, the PCM capsules have only point contacts with the tank wall, so the porosity of this position is close to 1, which means that the cylindrical surface is almost HTF, as shown in Fig. 8(a). At the position 0.5dp away from the wall, the cylindrical surface just passes through the center of the capsules, meaning that the PCM area will occupy most of the area of the cylindrical surface, and the porosity will be reduced to 0.15, as shown in Figure 8(b). Similarly, at the position dp away from the wall, the capsules near the wall are also in point contacts with the inner capsules. Gaps will be formed near the contact positions and the porosity becomes correspondingly larger with a value of 0.67, as shown in Fig. 8(c). Therefore, the cylindrical surfaces represented by the blue circles in Fig. 7a has a larger porosity than the cylindrical surfaces represented by the orange circles. As a result, the porosity on the cylindrical surface in the radial direction exhibits an oscillating distribution. But since the arrangement of capsules at the tank center is more random, this oscillating tendency will be gradually weakened, meaning that the wall effect on the internal porosity slowly decreases.

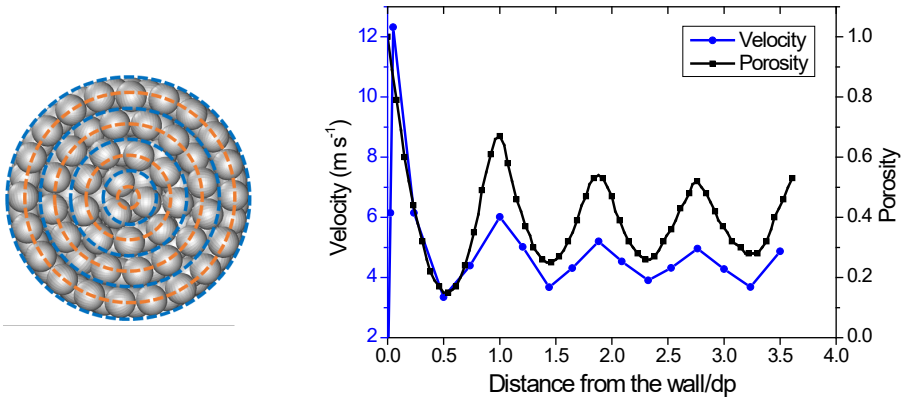

Fig. 7: a) Bottom view of the packed bed model; b) Radial porosity and velocity distribution in the packed bed

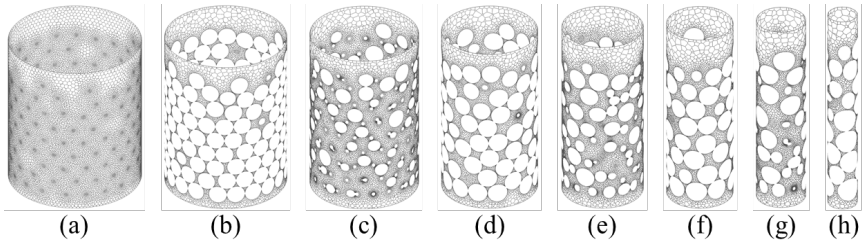

Fig. 8: Radial cylindrical surfaces inside the packed bed model (a-h represent the surfaces with the distance from the tank wall being 0, 0.5dp, dp, 1.44dp, 1.88dp, 2.32dp, 2.76dp, 3.24dp)

Accordingly, the velocity magnitude distributions of the HTF at different radial positions are shown in Fig.9, with the inlet mass flow rate being 260 kg • h^{-1}. The flow velocity of the HTF on the cylindrical faces a, c, e is

lower than that on the cylindrical faces b, d, f, which is the same as the porosity distribution on the cylindrical surfaces. The radial porosity distribution and velocity distribution are summarized in Fig. 7b, and it can be observed that at the wall, although the porosity is close to 1, the flow velocity is 0 due to wall viscosity. In the radial direction away from the wall, the velocity increases sharply and subsequently changes with the oscillation of the porosity. When the HTF enters the packed bed, it flows through the gaps between the PCM capsules. Locations with more gaps allow more HTF to flow through, thence the velocity of the HTF is faster where the porosity is larger.

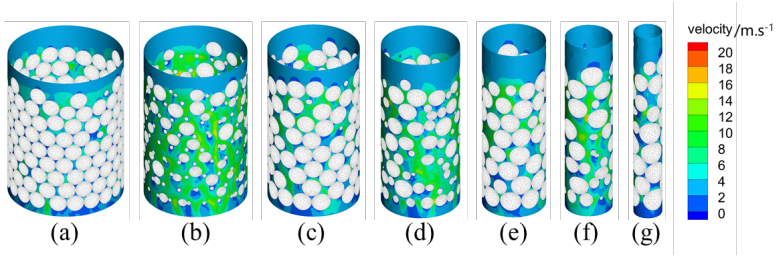

Fig. 9: Velocities of HTF at the radial cylindrical surfaces (a-g represent the surfaces with the distance from the tank wall being 0.5dp, dp, 1.44dp, 1.88dp, 2.32dp, 2.76dp, 3.24dp)

3.2 Heat transfer and heat storage analysis

In order to illustrate the changes of PCMs along the radial direction during the charging process, the temperatures and liquid fractions of the PCMs at the cylindrical surfaces mentioned above are calculated at different times, as shown in Fig. 11 and Fig. 12. The temperatures and liquid fractions of the PCMs fluctuate along the radial direction, in accord with the radial porosity distribution. The biggest fluctuation occurs at the near wall region, where HTF velocity fluctuates dramatically. At 600s, with temperatures reaching the melting point, the PCMs begin to melt and the liquid fractions increase. During phase transition temperature range, the PCMs need to absorb a large amount of heat to promote their temperatures. Therefore, although temperature differences of the PCMs on the cylindrical surfaces are small, the liquid fractions vary a lot. At 2400s, the liquid fractions all equal to 1 and the temperatures of the PCMs are almost the same, indicating that the charging process is about to finish. From the above, the velocity non-uniformity would cause temperature fluctuation, and the amplitude of the fluctuation gradually decays from the wall toward the center. In order to observe the heat storage of the PCMs on different cylindrical surfaces, the liquid fractions of PCMs at 600s are depicted in Fig. 13. It intuitively shows that PCMs melt faster on the surfaces with higher porosity, and PCMs near the HTF inflow side in the capsules melt faster.

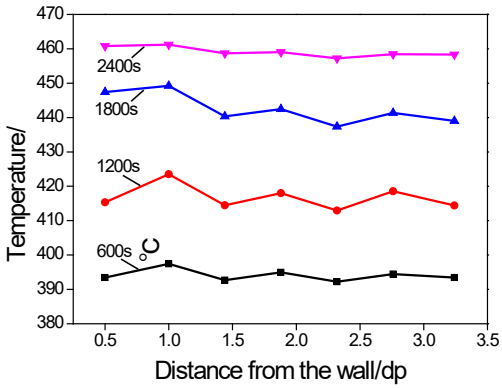

Fig. 11: Radial temperature evolutions of PCMs

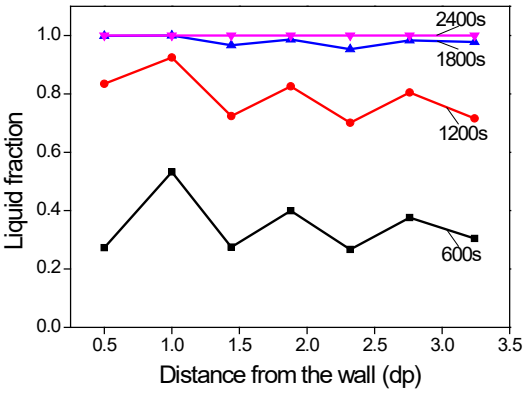

Fig. 12: Radial liquid fraction evolutions of PCMs

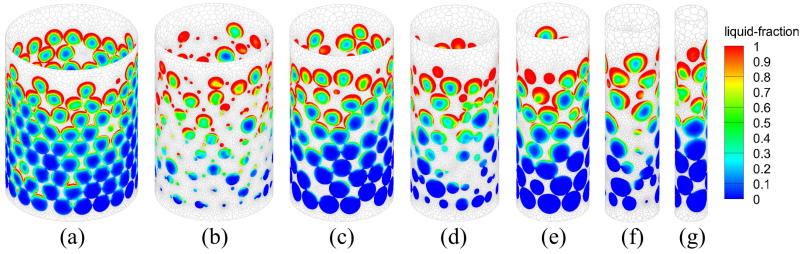

Fig. 13: Liquid fractions of PCMs at the radial cylindrical surfaces (a-g represent the surfaces with the distance from the tank wall being 0.5dp, dp, 1.44dp, 1.88dp, 2.32dp, 2.76dp, 3.24dp)

3.3 The effect of the aspect ratio

In this paper, the effect of different aspect ratios (4, 5, 6) on the flow, heat transfer and heat storage in packed bed LHS system are studied. The inlet and outlet boundary conditions remain unchanged, but the tank wall is set as adiabatic. The heat storage of the three packed bed LHS systems are designed to be almost the same, which is beneficial to further analysis and comparison. Based on this principle, the number of PCM capsules in the three packed beds is determined and summarized in Tab. 2. In Fig.14, the internal radial porosity distributions of the packed beds with different aspect ratios are compared, and it can be easily obtained that the radial porosity distributions all oscillate but have different trends. The radial porosity distributions are substantially same over a distance of 1.5 dp from the wall, but the closer to the center, the greater the differences. For the packed bed with the aspect ratio of 4, the diameter can be filled by 4 capsules, and capsules are in point contacts at the tank center, at which gaps are formed and consequently the porosity is large, as shown in Fig. 15a. For the packed bed with the aspect ratio of 5, the diameter can be filled by 5 capsules, thus the tank center is occupied by the capsules, and the central porosity is almost zero, as shown in Fig. 15b. For the packed bed with the aspect ratio of 6, the central porosity should be as large as that of the packed bed with an aspect ratio of 4 theoretically. However, since the tank center is a little far away from the tank wall, the influence of the wall is weakened, so the packing of capsules at the tank center tends to be random, which is consistent with the radial porosity distribution of the packed bed with the aspect ratio of 7.65.

Tab. 2: Parameters of the packed bed LHS systems with different aspect ratios

Tank	**Tank Diameter：240mm**	**Tank Height：500mm**
Ratio 4	**Capsule Diameter：60mm**	**Number of Capsules：105**
Ratio 5	**Capsule Diameter：48mm**	**Number of Capsules：205**
Ratio 6	**Capsule Diameter：40mm**	**Number of Capsules：354**
Thickness	**Tank Thickness：6mm**	**Shell Thickness：2mm**

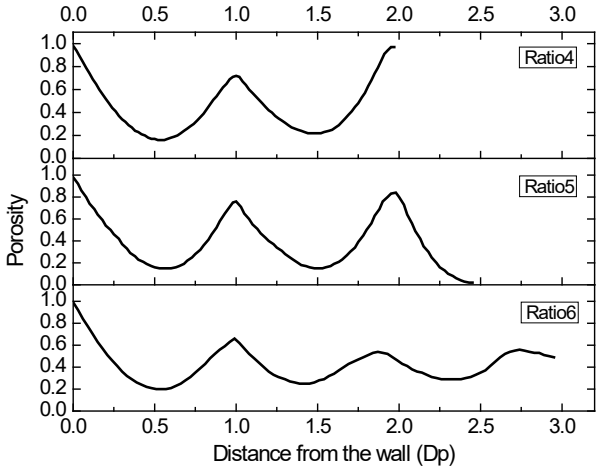

Fig. 14: Radial porosity distributions of the packed bed models with different aspect ratios

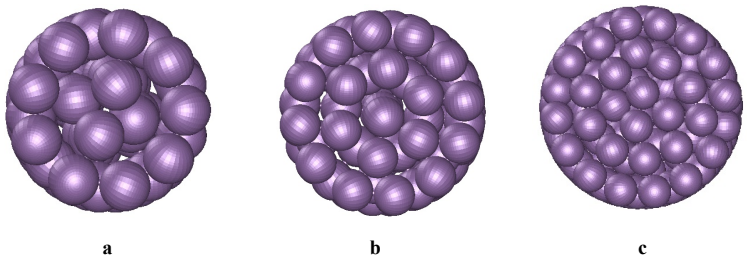

a b c

Fig. 15: Bottom view of the packed bed models with different aspect ratios: a) ratio 4, b) ratio 5, c) ratio 6

The flow velocity distributions inside the three packed bed LHS system models are illustrated in Fig. 16. It can be observed that the radial velocity distributions are consistent with the radial porosity distributions. However, the flow velocities near the wall in these packed beds are quite different. As the aspect ratio increases, the diameter of the PCM capsule decreases, so that the gaps formed near the contact points between the capsules and the container wall are smaller. For the hot air with the same mass flow rate, the flow velocity will be larger at the gaps near the wall accordingly. Further, the radial liquid fraction distributions of the packed beds when t = 1200s are shown in Fig. 17, which are basically consistent with the radial porosity distributions. Wherein for the packed bed with the aspect ratio of 6, the heat storage process of the PCM in the capsules near the wall is faster than that at the tank center because the flow rate near the wall is far larger.

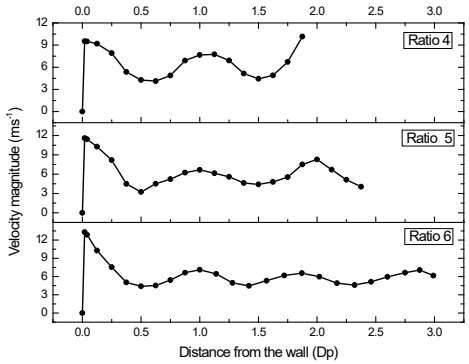

Fig. 16: Radial flow velocity distributions of the packed bed LHS systems with different aspect ratios

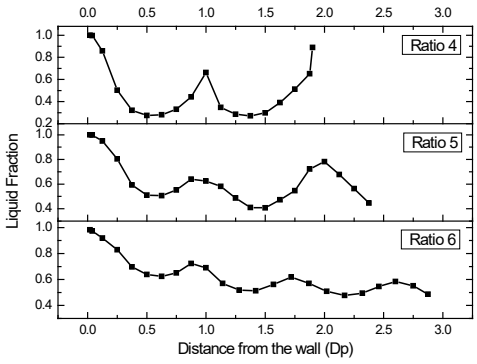

Fig. 17: Radial liquid fraction distributions of the packed bed LHS systems with different aspects ratio at 1200s

The total heat storage in the packed bed LHS system includes the heat stored in the PCM, the PCM capsule shells, and the heat stored in the tank wall. Among them, the heat stored in the PCM includes the sensible heat in the solid state and liquid state, as well as the latent heat during phase change, while the heat stored in the PCM capsule shells and the tank is sensible heat. Hence the total heat storage in the packed bed LHS system can be expressed as:

$$Q_{\text{total}} = Q_{\text{pcm}} + Q_{\text{shell}} + Q_{\text{tank}} \quad \text{(eq.16)}$$

$$Q_{\text{pcm}} = m_{\text{pcm}}[C_{\text{p,s}}(T_{\text{m}} - T_0) + \Delta H + C_{\text{p,l}}(T_{\text{in}} - T_{\text{m}})] \quad \text{(eq.17)}$$

$$Q_{\text{shell}} = m_{\text{shell}} C_{\text{p,shell}}(T_{\text{in}} - T_0) \quad \text{(eq.18)}$$

$$Q_{\text{tank}} = m_{\text{tank}} C_{\text{p,tank}}(T_{\text{in}} - T_0) \quad \text{(eq.19)}$$

During the charging process, heat storage of the packed bed LHS system can be obtained by the first law of thermodynamics:

$$Q_{\text{stored}} = \int \dot{m}_{\text{f}}(c_{\text{pf,in}} T_{\text{f,in}} - c_{\text{pf,out}} T_{\text{f,out}})\text{d}T \quad \text{(eq.20)}$$

Therefore, the charging efficiency of the system during charging process is defined as:

$$\eta_{\mathrm{charge}} = \frac{Q_{\mathrm{stored}}}{Q_{\mathrm{total}}} \quad \text{(eq.21)}$$

The average charging power can be defined as (Li et al., 2018a):

$$P_{\mathrm{aver}} = \frac{Q_{\mathrm{stored}}}{\tau_{\mathrm{charge}}} \quad \text{(eq.22)}$$

In Fig.18, heat storage and the average charging power of the packed bed LHS systems with different aspect ratios are calculated. As the aspect ratio increases, the average charging power of the packed bed LHS systems are increased. Furthermore, the charging time decreases with the increase of aspect ratio, and the charging time of the three systems are 121.03 min, 89.73 min, and 79.80 min respectively, as shown in Fig.19. It can be obtained that the results of the system with the aspect ratio of 4 differ a lot from those of the system with the aspect ratio of 5 and 6. The reason is that the capsule diameter of the system with the aspect ratio of 4 is 60 mm, while capsules in systems with the aspect ratios of 5 and 6 have diameters of 48 mm and 40mm, accordingly the heat transfer distance is 80% and 66.67% of 60mm. Only considering the charging time and average charging power, the system with the aspect ratio of 5 or 6 is more suitable for applications than the system with the aspect ratio of 4. However, as the aspect ratio increases, the pressure drop within the packed bed LHS system also increases rapidly, as shown in Fig.19. Therefore, when the packed bed LHS system is considered to be used in practical situations, it is necessary to comprehensively consider the charging time, the charging power, as well as the pressure drop.

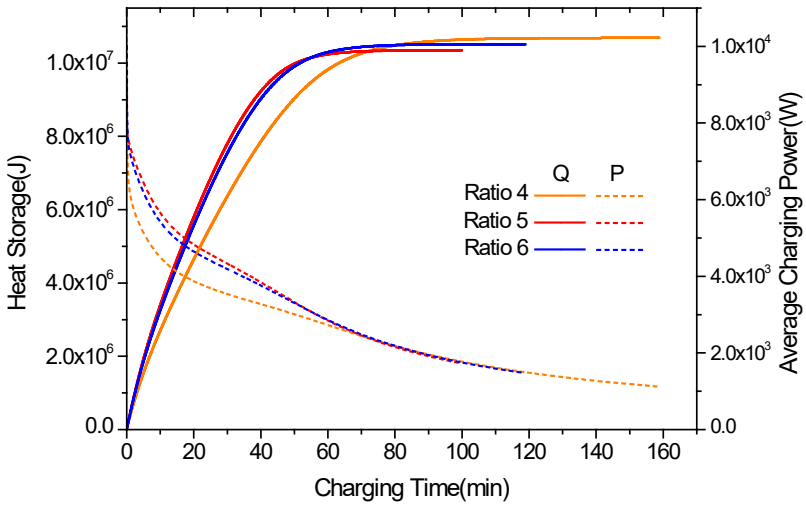

Fig. 18: Heat storage and the average charging power of the packed bed LHS systems with different aspect ratios

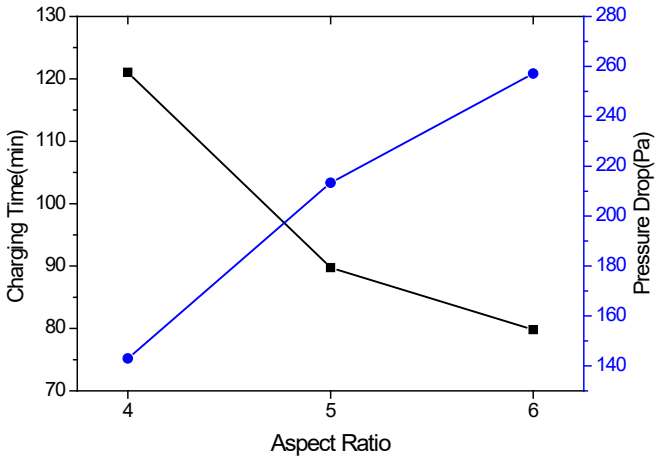

Fig. 19: Charging time and pressure drop of the packed bed LHS system with different aspect ratio

4. Conclusion

In this paper, the necessity of establishing a three-dimensional packed bed LHS model is proposed by analyzing the existing numerical methods of packed bed. The three-dimensional packed bed LHS model is constructed by programming in Blender, and the internal radial porosity distribution of the model has a high degree of agreement with the experimental data. Moreover, the accuracy of the model is further verified by comparison with experimental results during the charging process. The reason why radial porosity shows an oscillation distribution is demonstrated by intercepting different cylindrical faces along the radial direction. Porosity changes sharply near the wall, while the change of porosity near the tank center is more moderate. The oscillating distribution of radial porosity leads to the non-uniform flow velocity distribution and then further affects the heat transfer in the packed bed. The velocity distribution of HTF and the temperature distribution of PCMs are consistent with the distribution of porosity. Therefore, PCMs melt faster at the positions with higher porosity. In addition, the effect of different aspect ratios (4, 5, 6) on the flow, heat transfer and heat storage in the packed bed LHS system are studied. The radial porosity of the packed beds with different aspect ratios shows different distributions, and the closer to the center position, the greater the difference. As the aspect ratio increases, the packing of PCM capsules at the tank center becomes more random. Furthermore, the flow velocity of the HTF near the wall also increases, which results in a faster heat transfer and charging rate of the PCM capsules at the near wall region. Finally, when the aspect ratio increases, the diameter of the PCM capsule is greatly reduced, so the charging time can be greatly reduced, and the average charging power can be also improved. However, the pressure drop within the packed bed LHS system increases with the increase of the aspect ratio. It is significant to comprehensively consider the charging time, the charging power, as well as the pressure drop, when the packed bed LHS system is applied to practical situations.

5. Acknowledgments

This work is supported by the National Key Basic Research Program of China (973 Project: 2013CB228303) and the National Natural Science Foundation of China (Grant No.51906150).

6. References

Alam, T.E., Dhau, J.S., Goswami, D.Y., Stefanakos, E., 2015. Macroencapsulation and characterization of phase change materials for latent heat thermal energy storage systems. Applied Energy 154, 92-101.

Anderson, R., Bates, L., Johnson, E., Morris, J.F., 2015. Packed bed thermal energy storage: A simplified experimentally validated model. Journal of Energy Storage 4, 14-23.

Argyropoulos, C.D., Markatos, N.C., 2015. Recent advances on the numerical modelling of turbulent flows. Applied Mathematical Modelling 39(2), 693-732.

Bellan, S., Alam, T.E., González-Aguilar, J., Romero, M., Rahman, M.M., Goswami, D.Y., Stefanakos, E.K., 2015. Numerical and experimental studies on heat transfer characteristics of thermal energy storage system packed with molten salt PCM capsules. Applied Thermal Engineering 90, 970-979.

Dixon, A.G., Nijemeisland, M., Stitt, E.H., 2013. Systematic mesh development for 3D CFD simulation of fixed beds: Contact points study. Computers & Chemical Engineering 48, 135-153.

Eppinger, T., Seidler, K., Kraume, M., 2011. DEM-CFD simulations of fixed bed reactors with small tube to particle diameter ratios. Chemical Engineering Journal 166(1), 324-331.

Freund, H., Zeiser, T., Huber, F., Klemm, E., Brenner, G., Durst, F., Emig, G., 2003. Numerical simulations of single phase reacting flows in randomly packed fixed-bed reactors and experimental validation. Chemical Engineering Science 58(3-6), 903-910.

Gunjal, P.R., Ranade, V.V., Chaudhari, R.V., 2005. Computational study of a single-phase flow in packed beds of spheres. AIChE Journal 51(2), 365-378.

Li, M.-J., Jin, B., Ma, Z., Yuan, F., 2018a. Experimental and numerical study on the performance of a new high-temperature packed-bed thermal energy storage system with macroencapsulation of molten salt phase change material. Applied energy 221, 1-15.

Li, M.-J., Jin, B., Yan, J.-J., Ma, Z., Li, M.-J., 2018b. Numerical and Experimental study on the performance of a new two-layered high-temperature packed-bed thermal energy storage system with changed-diameter macro-encapsulation capsule. Applied Thermal Engineering 142, 830-845.

Mueller, G.E., 1992. Radial void fraction distributions in randomly packed fixed beds of uniformly sized spheres in cylindrical containers. Powder technology 72(3), 269-275.

Mueller, G.E., 2005. Numerically packing spheres in cylinders. Powder technology 159(2), 105-110.

Mueller, G.E., 2010. Radial porosity in packed beds of spheres. Powder Technology 203(3), 626–633.

Partopour, B., Dixon, A.G., 2017. An integrated workflow for resolved-particle packed bed models with complex particle shapes. Powder Technology 322, 258-272.

Xia, L., Zhang, P., Wang, R.Z., 2010. Numerical heat transfer analysis of the packed bed latent heat storage system based on an effective packed bed model. Energy 35(5), 2022-2032.

Yakhot, V., Smith, L.M., 1992. The renormalization group, the ε-expansion and derivation of turbulence models. Journal of Scientific Computing 7(1), 35-61.

Zhang, H.L., Baeyens, J., Caceres, G., Degreve, J., Lv, Y.Q., 2016. Thermal energy storage: Recent developments and practical aspects. Prog. Energy Combust. Sci. 53, 1-40.

Zhao, B., Cheng, M., Liu, C., Dai, Z., 2017. An efficient tank size estimation strategy for packed-bed thermocline thermal energy storage systems for concentrated solar power. Solar Energy 153, 104-114.

Zhao, Y., You, Y., Liu, H., Zhao, C., Xu, Z., 2018. Experimental study on the thermodynamic performance of cascaded latent heat storage in the heat charging process. Energy 157, 690-706.